

We are IntechOpen, the world's leading publisher of Open Access books Built by scientists, for scientists

4,800

Open access books available

122,000

International authors and editors

135M

Downloads

Our authors are among the

154

Countries delivered to

TOP 1%

most cited scientists

12.2%

Contributors from top 500 universities



WEB OF SCIENCE™

Selection of our books indexed in the Book Citation Index
in Web of Science™ Core Collection (BKCI)

Interested in publishing with us?
Contact book.department@intechopen.com

Numbers displayed above are based on latest data collected.
For more information visit www.intechopen.com



Design of Reconfigurable Multiple-Beam Array Feed Network Based on Millimeter-Wave Photonics Beamformers

*Mikhail E. Belkin, Dmitriy A. Fofanov,
Tatiana N. Bakhvalova and Alexander S. Sigov*

Abstract

In this chapter, elaborating the direction of designing photonics-based beamforming networks (BFN) for millimeter-wave (mmWave) antenna arrays, we review the worldwide progress referred to designing multiple-beam photonics BFN and highlight our last simulation results on design and optimization of millimeter-photonics-based matrix beamformers. In particular, we review the specialties of mmWave photonics technique in 5G mobile networks of Radio-over-Fiber (RoF) technology based on fiber-wireless architecture. In addition, the theoretical background of array antenna multiple-beam steering using ideal models of matrix-based phase shifters and time delay lines is presented including a general analysis of radiation pattern sensitivity to compare updated photonics beamforming networks produced on phase shifter or true-time delay approach. The principles and ways to optimized photonics BFN design are discussed based on the study of photonics BFN scheme including integrated 8×8 optical Butler matrix (OBM). All schemes are modeled using VPIphotonics Design Suite and MATLAB software tools. In the result of simulation experiments, the outcome is obtained that both the integrated optical Butler matrix itself and the BFN based on it possess an acceptable quality of beams formation in a particular 5G pico-cell.

Keywords: 5G mobile communication network, small cell, wideband millimeter-wave antenna array, photonics-based beamforming network, computer-aided design

1. Introduction

Generally, antenna unit is a requisite of any on-air radio frequency system forming its service area and bandwidth capability. At present, implementing an active phased array antenna (PAA) [1] results in remarkably increased footprint and operation flexibility thanks to electronic beam steering function, which is realized by a beamforming network (BFN). Today, the global telecommunications industry is experiencing a stage of violent development associated with the becoming of the fifth-generation mobile communication networks (5G NR) [2–6], and it is planned that one of the milestones for 5G NR compared to available 4G LTE networks should be millimeter-wave (mmWave) communication with mobile radio

terminals [7, 8]. This approach should lead to a newer network design technology using Radio-over-Fiber (RoF) building concept as well as PAA-assisted remote stations (RS) and user terminals (UT) [8, 9]. On this way, integrated and millimeter-wave (mmWave) photonics are extremely attractive technologies for realizing a PAA's interactive optical BFN due to its superior instantaneous operating bandwidth, immunity to electromagnetic interference, lightweight, and reconfigurability [3].

Following it, recently we designed photonics-based BFNs for ultrawide bandwidth mmWave (57–76 GHz) antenna arrays [10]. Elaborating the direction, in this chapter, we review the worldwide progress referred to designing multiple-beam photonic BFN and highlight our last simulation results on design and optimization of millimeter-photonics-based matrix beamformers. Thus, in the rest of the sections, the following topics are under consideration. In particular, Section 2 reviews the specialties of mmWave photonics technique in 5G mobile networks of RoF technology based on fiber-wireless (FiWi) architecture. In addition, Section 3 presents theoretical background of array antenna multiple-beam steering using ideal models of matrix-based phase shifters and time delay lines. Section 4 includes a general analysis of radiation pattern sensitivity to compare updated photonics beamforming networks produced on phase shifter or true-time delay (TTD) approach. The principles and ways to optimized photonics BFN design are discussed in Section 5 based on the photonics BFN scheme including integrated 8×8 optical Butler matrix (OBM). All schemes are modeled using VPIphotonics Design Suite and MATLAB software tools. Finally, Section 6 concludes the chapter.

2. Millimeter-wave photonics technique in 5G fiber-wireless networks

Based on 4G LTE progress [3], 5G NR is in principle a novel stage of unprecedented technological innovation with ubiquitous speed connectivity. As a result, it is expected that 5G NR will radically transform a number of industries and will provide direct, super-speed connections between any users and any sensors and devices. By now, several reviews to analyze significant changes in the 5G NR approaches as compared to the existing 4G LTE networks have been published [8, 11] denoting a series of milestones. Developing this topic, **Table 1** summarizes the results of the advanced analysis focusing on the investigations referred to a fronthaul network with mobile communication in mmWave-band.

The review of the current R&Ds in 5G NR area convincingly demonstrates the consistent achievement of the designated in **Table 1** milestones, which is reflected in a vast number of publications and emergence of commercial products. Among them, much attention is paid to radically expanding the available spectral bands up to mmWaves (see item 1 of **Table 1**) to promote the throughput of mobile communication system. Following this tendency, currently, the local telecommunications commissions of various countries are proposing and harmonizing the plans of frequency allocation in mmWave-band, which will be reviewed this year at the World Radio Conference (WRC-2019). Currently, for the 5G NR networks, it is planned to allocate two frequency bands (see **Figure 1**), coexisting with available 4G LTE systems in the 1–6 GHz band (the so-called “low range” (LR)) and new one in the mmWaves within the range of 24.5–86 GHz according to [12] (the so-called “high range” (HR)).

Based on various investigations, let us review the key advantages and disadvantages of the mobile communication system operation in the millimeter range. The following are the advantages of the 5G mmWave mobile communication:

- It provides larger bandwidth, and hence, more number of UT can be accommodated.
- Its coverage is not limited to the line of sight (LoS) as first-order scatter paths are viable.
- Channel sounding feature is employed to take care of different types of losses at mmWave frequencies so that 5G network operates satisfactorily thanks to the measurement or estimation of channel characteristics, which helps in successful design, development, and deployment of 5G network with necessary quality requirements.
- Antenna size is physically small, and hence, a large number of antennas are packed in small volume. This leads to the use of massive multiple input, multiple output (MIMO), or beam-steerable PAA in RS to enhance the capacity (see item 2 of **Table 1**).

No.	Designation	Short description
1	Radically expanding the available spectral bands	Some superwide bandwidth cases in 5G access networks will require contiguous carrier bandwidths. To support them, additional carrier frequencies (below 6 GHz), as well as mmWave RF carriers will be required
2	Using active antenna systems in mmWave communication	Following the tendencies of expanding the available spectral bands and increasing user densification, mmWave 5G wireless network infrastructure can be erected with a lot of small cell sites controlled by the corresponding RSs. In order to avoid inter-interference inside these cells, one of the promising approaches is to equip the RS with beam-steerable PAA using hundreds of antenna elements to form multiple directional beams in omnidirectional space
3	Establishing optimized access network architecture	Following the milestone of item 1, it is necessary to optimize the access network architecture so that at the same time it will provide high-quality communication with fixed and mobile users subject to low charges for the building and maintenance of networks. A promising candidate for solving the problem is a RoF's FiWi architecture, already tested in 4G LTE systems

Table 1.
 The milestones in the way to transform 4G LTE to 5G NR.

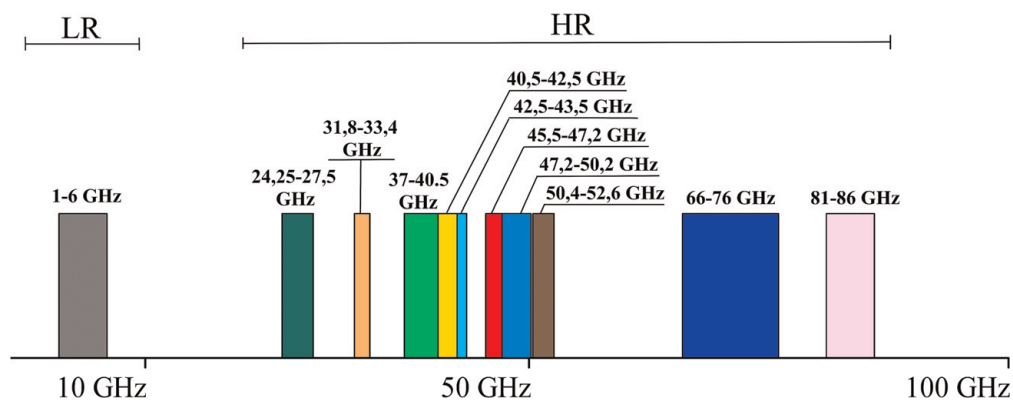


Figure 1.
 Planned 5G NR spectrum allocations [12].

- Dynamic beamforming is employed, and hence, it mitigates higher path loss at mmWave frequencies.
- 5G mmWave networks support multi-gigabit backhaul up to 400 m and cellular access up to 200–300 m [13].

Due to these benefits, 5G mmWave is suitable for mobile communication over sub-6 GHz wireless technologies. The main disadvantages of 5G mmWave communication are the next:

- Millimeter-wave goes through different severe losses such as penetration, rain attenuation, and even foliage. This limits distance coverage requirement in 5G-based cellular mobile deployment. Moreover, path loss is proportional to the frequency squared. It supports about 200–300 m in outdoors based on channel conditions and RS antenna height above the ground.
- It supports only LoS that limits the cell coverage.
- Power consumption is higher due to the greater number of RF modules and antennas. To avoid this drawback, hybrid architecture, which has fewer RF chains than the number of antennas, needs to be used at the RS receiver chain.

These disadvantages must be considered during 5G mmWave link budget calculation.

The drawbacks mentioned above led to the need for a radical change in the architecture of access networks compared to 4G LTE. In particular, instead of macro-cells, a multistage configuration was introduced, additionally containing micro-cells and pico-cells [3, 14]. In this direction, a newer RoF-based access networks of FiWi architecture is considered as the most promising approach (see item 3 of **Table 1**) ([9, 11]). The reason is that the important drawback for the implementation of the wired links, for example, of Fiber-to-the-Home (FTTH) architecture is feasible for fixed UTs only. In contrast, current wireless access networks of 4G LTE that provide a flexible communication with a relatively simple infrastructure cannot meet growing in geometric progression demands to increase the capacity of mobile systems. The most promising technique to meet it, which is actively discussed in the referred publications, is to expand the operating frequency band and to apply multi-position digital modulation of a radio frequency (RF) carrier through fiber fronthaul to simplify pico-cell RS layout. **Figure 2** illustrates a typical pico-cell in a large city. The mmWave wireless network is managed from a remote station including one unidirectional PAA for downlink and uplink channels.

2.1 The outcome

The source data for posterior calculations of multi-beam PAA in a pico-cell are:

- The base station is located on a separate mast of 3 m high in the geometric center of the service area (see **Figure 2**).
- The overall azimuth angle for the PAA under study is 360°.
- The elevation angle for the PAA under study must be such that the dead area around the mast does not exceed 1 m.



Figure 2.
Sketch of a typical wireless pico-cell for 5G access network.

- The service radius of the pico-cell under investigation is 50 m.
- The operating frequency band is 37.0–43.5 GHz (see **Figure 1**).

3. Theoretical background of multiple-beam array antenna beam steering

As noted in chapter 2, mmWave array antennas capable of operating in ultrawide frequency range are considered as one of the key enabling technologies for designing RS of 5G NR network. There, a formation of a narrow steered beam by means of a PAA makes it possible to increase the directive gain to compensate for the excessive loss in the mmWave-band. Besides, the use of narrow beams would reduce the interference effects from other closely spaced mobile terminals and provides the possibility of spatial multiplexing to increase throughput while simultaneously exchanging information with several RSs.

Generally, electronic scanning in the PAA is provided by a beamforming network, which includes phase shifters or delay lines [1]. The BFN supports a continuous or discrete beam movement in space due to phase control or signal delay between the array elements. In our previous work devoted to the study of the PAA BFN [10], a single-beam PAA with electronic scanning of the radiation pattern was considered. Nevertheless, for 5G pico-cells in conditions of simultaneous communication with a large number of terminal units, using a set of multiple-beam antenna (MBA) is considered to be a more practical way. PAAs based on MBA have greater functionality, but they are very complex, bulky, energy-consuming, and expensive devices. These factors limit their use to date mainly in special-purpose radars and unique satellite communication stations, for example, in satellite arrays of the iridium global mobile communication system [15]. There, PAA of the transponder has 106 channels and forms 16 fixed beams covering the contour-shaped

the Earth's area. Each satellite has three such PAA, each of which forms its own sector. Thus, a set of 48 fixed satellite beams covers the Earth's area of about 4000 km in diameter.

As noted in [10], an appropriate beamforming scheme focusing the transmitted and/or received signal in a desired direction in order to overcome the unfavorable path loss is one of the key enablers for cellular communications in mmWave frequency bands. Depending on its layout, the beamforming weights required to form the directive beam could be applied in the digital or analog domain. Generally, digital beamforming provides a higher degree of freedom and offers better performance at the expense of increased complexity and cost because separate digital-to-analog converters, and analog-to-digital converters are required per each RF chain. Analog beamforming, on the other hand, is a simple and effective method of generating high beamforming gains from a large number of antennas but less flexible than digital counterpart.

For analog MBAs, BFN on the basis of multipole microwave circuits are usually applied. In particular, multipoles based on the Butler and Blass schemes are in common use since they are more compact than quasi-optical BFNs. In addition, they can be performed on printed circuit boards decreasing BFN's cost, size, weight, and power (C-SWaP) characteristics that are critical challenges in communication system design. For example, Butler matrix-based BFNs are exploited in the abovementioned iridium system. Currently, fixed-beam PAAs that use matrix BFNs based on a parallel circuitry (Butler matrix) and a serial circuitry (Blass matrix) [1] are being developed for photonics compatible mmWave small cell RSs of incoming 5G NR mobile communication networks.

Following this, below, a short theoretical study using ideal models is presented pursuing the goal to define the optimum RS's omnidirectional antenna construction, type, and configuration of multi-beam matrix for its BFN and the input data for the posterior design and optimization of the specific photonics-based BFN for the mmWave-band PAA exploiting widespread computer-aided design (CAD) tools.

First, following [1], the schematics and characteristics of Butler and Blass matrixes are discussed below.

3.1 Butler matrix

The traditional RF-band layout of Butler matrix consists of quadrature hybrids, fixed phase shifters, and transmission lines between them. A matrix can be used to feed a PAA; the number of elements of which is a multiple of degree 2. **Figure 3**

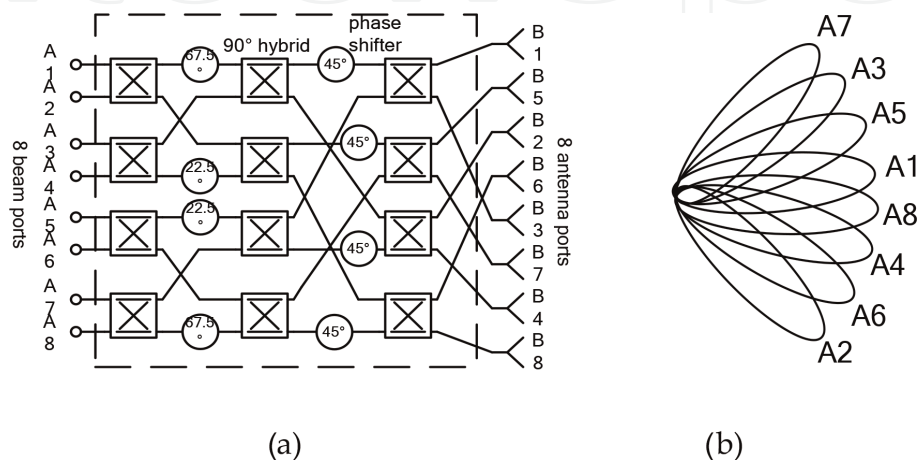


Figure 3.
(a) Block diagram of 8x8 traditional Butler matrix and (b) corresponding BFN beam rosette.

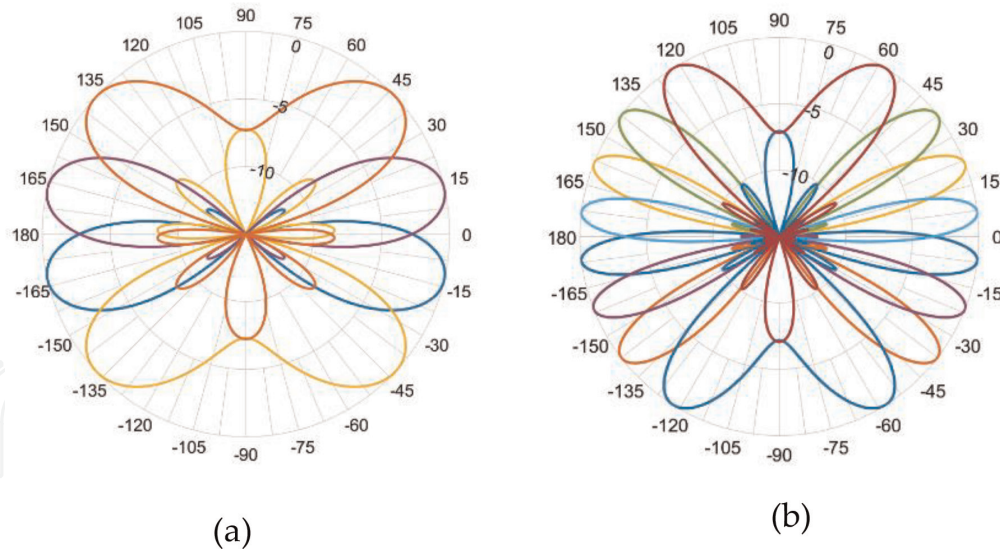


Figure 4.
 Examples of the normalized radiation patterns for 4×4 (a) and 8×8 (b) Butler matrix.

demonstrates the block diagram (a) and BFN beam rosette (b) of the 8-element Butler matrix.

The number of inputs of the matrix is equal to the number of outputs. The amplitude-phase distribution at the outputs of the Butler matrix is described by the following formula:

$$A_n = \frac{1}{\sqrt{N}} \sum_{m=1}^N e^{-j\frac{2\pi}{N}(m-1)(n-1)} \quad (1)$$

where N is the number of channels; m and n are the number of the inputs and outputs, respectively. It should be noted that Eq. (1) is essentially a fast Fourier transform.

When connected to a linear equidistant PAA of N omnidirectional element, the Butler matrix forms N orthogonal beams, symmetrically located relative to the normal, with maxima in the azimuth directions φ_i measured from the PAA broadside and determined by the formula:

$$\cos \varphi_i = \left(i - \frac{N+1}{2} \right) \frac{\lambda}{L}, \quad i = \overline{1..N}, \quad (2)$$

where λ is the operating wavelength and L is the PAA aperture. Moreover, the beams intersect each other at a level of -4 dB. As it follows from Eq. (2), the direction of the beams deviates when λ varies, that is, a so-called squint effect is observed. Besides, the fan of orthogonal beams shrinks with decreasing λ/L that is clearly seen in **Figure 4** illustrating the normalized radiation patterns (NRP) for 4×4 (a) and 8×8 (b) Butler matrix calculated by MATLAB software.

Thus, due to the simplicity of the design and a relatively small number of elements, the Butler matrix is used in tasks that do not require the possibility of arbitrarily setting beam directions, for example, in covering the wide service sector of a wireless system.

3.2 Blass matrix

The Blass matrix consists of directional couplers connected to the inputs and outputs using transmission lines with different fixed delays. The matrix can be used to supply signals to the PAA with an arbitrary number of elements; the number of

inputs can also be arbitrary and is determined by the required number of beams to be formed. The block diagram of the Blass matrix for three inputs and eight outputs, as well as the BFN beam rosette is shown in **Figure 5**.

The amplitude-phase distribution at the outputs of the Blass matrix with N inputs is determined by the delays of the transmission lines τ_{mn} and the levels of the signals branched off each of the directional couplers a_{mn} according to the formula:

$$A_n = \sum_{m=1}^N a_{mn} e^{-j\omega\tau_{mn}}, \quad (3)$$

where m is the input number n is the output number.

Due to the fact that the RF signal from the input port sequentially passes through several directional couplers for feeding all the PAA elements, each coupler in the matrix must have the strictly defined value of the branch ratio, which greatly complicates the design. The configuration of the Blass matrix requires a larger number of directional couplers than Butler matrix, which increases its cost and often degrades the C-SWAP characteristics. However, due to the use of delay lines, the beams do not deviate from their position when the wavelength λ varies as it happens using the Butler matrix (see Eq. (2)). For this reason, the Blass matrix is better feasible for ultrawide band systems with a fractional bandwidth of more than 20%, as well as in systems requiring specific beam placement, for example, in satellite broadcasting equipment. Based on this outcome, in the course of further consideration of 5G mmWave MBA beam steering, only the BFN based on the Butler matrix will be studied.

3.3 Antenna system for a mmWave pico-cell remote station of 5G mobile communication network

From the outcome of Section 1, it follows that using an antenna's installation height of 3 m and a coverage radius of 50 m, the elevation angle of 78° , provided by a half-wave dipole in the E-plane, is sufficient to provide a radius of not more than 0.5 m for the dead zone in the immediate vicinity of the mast (see **Figure 6**).

As can be seen in **Figure 4**, the extreme beams generated by the Butler matrix have a significantly greater width and less directivity than the others do. Their use

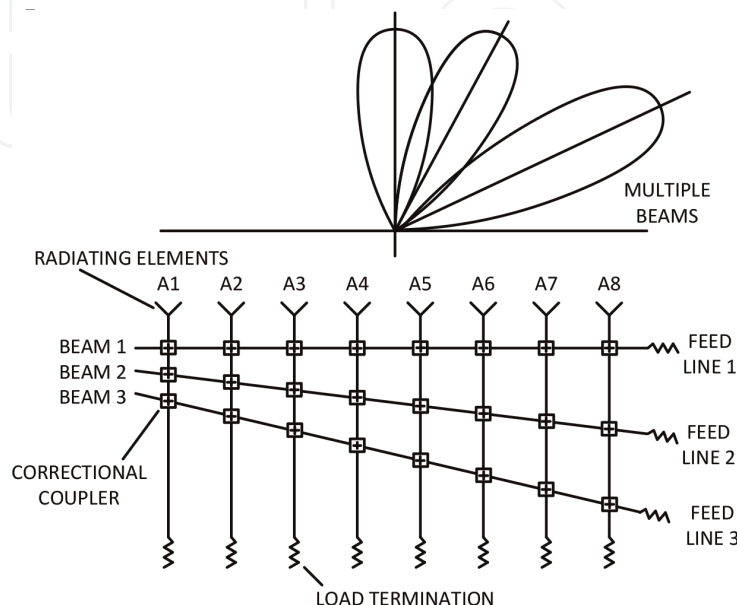


Figure 5. Block diagram of the 3×8 Blass matrix (bottom) and corresponding BFN beam rosette (top).

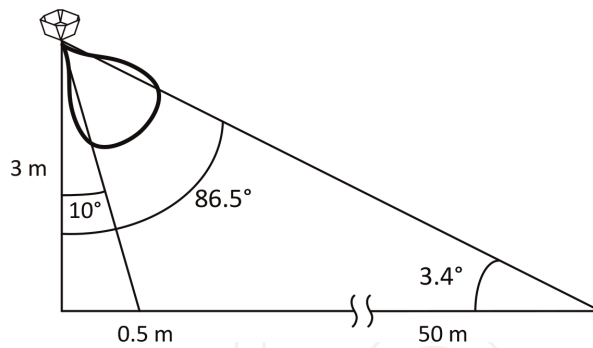


Figure 6.
 Calculation of the radiation pattern in the elevation plane for one-dimensional PAA.

should be abandoned in order to avoid creating significant interference outside the service sector. Thus, the 4×4 matrix makes it possible to effectively exploit only two beams, which is not enough for spatial multiplexing of communication channels under the conditions illustrated in **Figure 2**; it is necessary to use an 8×8 matrix with six active channels. A fan using six beams allows covering a sector of the order of 50° for the -4 dB level (see **Figure 4**), which provides a full 360° coverage with four PAAs mounted at 90° relative to each other, as shown in **Figure 7**.

According to [1], the radiation pattern of a PAA $D(\theta, \varphi)$ is determined by the radiation pattern of a single antenna element $f(\theta, \varphi)$ and the array factor $F(\theta, \varphi)$ by the formula

$$D(\theta, \varphi) = f(\theta, \varphi) * F(\theta, \varphi), \quad (4)$$

where θ is an elevation angle and φ is an azimuth.
 For a half-wave dipole,

$$\begin{aligned} f(\theta, \varphi) &= f(\theta) * f(\varphi) \\ f(\varphi) &= \text{const}, \\ f(\theta) &= \frac{1 + \cos(\pi \cos \theta)}{\sin \theta} \end{aligned} \quad (5)$$

For a one-dimensional linear equidistant 8×1 PAA with a distance between elements $d = \lambda_0/2$

$$\begin{aligned} F(\theta, \varphi) &= F(\theta) * F(\varphi) \\ F(\theta) &= \text{const}, \\ F(\varphi) &= \sum_{n=1}^8 A_n e^{j \frac{2\pi f}{c} n \frac{\lambda_0}{2} \cos \varphi}, \end{aligned} \quad (6)$$

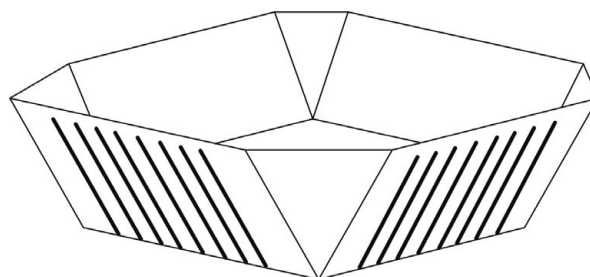


Figure 7.
 Configuration of the antenna system for the mmWave pico-cell remote station under study.

where f is the signal frequency inside the operating frequency range of 37–43,5 GHz, c is the light speed in vacuum, λ_0 is the wavelength corresponding to the center frequency of the operating frequency range, and A_n is amplitude-phase distribution generated by the Butler matrix and determined according to Eq. (2). Thus, the six-beam radiation pattern of single PAA is described by the formula:

$$D(\theta, \varphi) = \frac{1 + \cos(\pi \cos \theta)}{\sin \theta} * \sum_{n=1}^8 \left[\frac{1}{\sqrt{8}} \sum_{m=1}^6 e^{-j\frac{2\pi}{N}(m-1)(n-1)} \right] e^{j\frac{2\pi f}{c} n \frac{\lambda_0}{2} \cos \varphi} \quad (7)$$

Equation (7) is fundamental for further modeling.

Note that to ensure the required coverage in the elevation plane, the PAA panels have to be tilted to the ground at an angle near 45°. The unidirectional coverage provided in the azimuth plane by four sub-arrays of antenna system is illustrated in **Figure 8**.

To summarize, the following outcomes could be concluded:

- The Butler matrix is more suitable for the formation of a multipath radiation pattern in comparison with the Blass matrix because of its simpler design, fewer components, and better C-SWAP characteristics.
- The use of six central beams, generated by the eight-channel Butler matrix, provides a coverage sector of about 50° and does not create a significant level of interference beyond its limits.
- The omnidirectional coverage of the service area is provided by using half-wave dipoles as elements of the one-dimensional PAA, providing coverage of 78° in elevation angle and an antenna system of four linear PAA, providing overall coverage of 360° in azimuth.

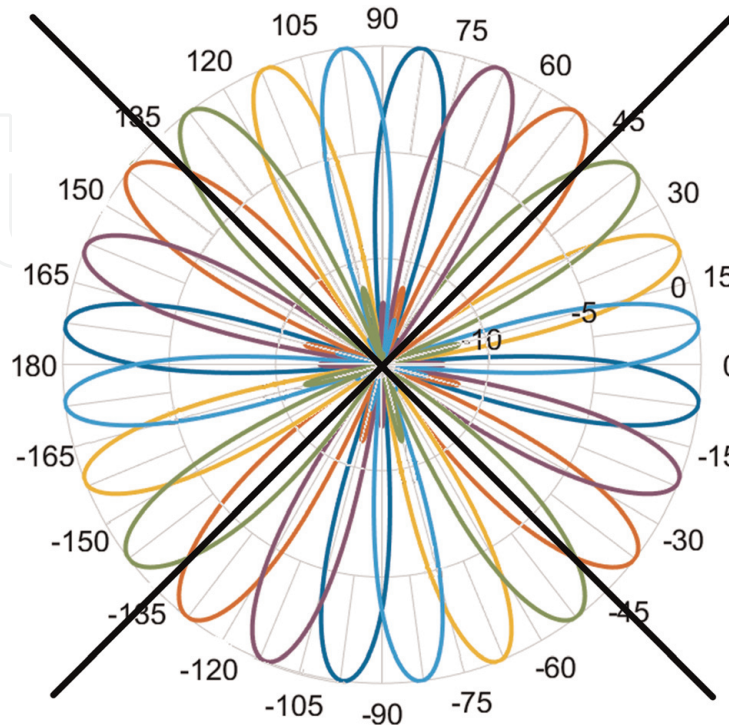


Figure 8.
Radiation pattern of RS antenna system in the azimuth plane.

4. A general analysis of radiation pattern sensitivity

Due to the difficulty in providing time delays between PAA elements, phase shifters usually control the steering signal instead of using actual time delays, because their realization in RF band is much simpler, especially in the case of limited bandwidth. However, a phenomenon called “beam squint” leads to an error in the direction of the maximum of the PAA pattern and also to a certain increase in the level of the side lobes. Nevertheless, as known, a BFN based on phase shifters has become widespread in relatively narrowband RF-band PAAs with a fractional bandwidth, commonly not exceeding 10%, depending on the criterion used [16]. Though, the development of a key trend for 5G NR networks associated with the implementing the mmWave in the wireless frontend has led to a change in the design principle of the access network’s RS, whose antenna pattern was steered using photonics technique. At the same time, due to the more complexity for the implementation of fundamentally narrowbandwidth phase shifters in the optical range, the so-called true -time delay (TTD) concept based on wideband optical delay lines has been widely used [17–20].

Thus, when the fractional bandwidth of the BFN under design exceeds the 10% as noted above, it is required to determine the optimal approach by analyzing the sensitivity of the radiation pattern to the frequency change in the entire specific RF range. We previously performed this procedure for the mmWave PAA with single-beam photonics BFN operating in the 57–76 GHz RF band (fractional bandwidth of 28.6%) [10]. As a result of the direct comparison, the TTD approach was unambiguously selected, since using phase shifters in the BFN produced more than 10% shift in the azimuth angle for the main lobe of the NRP, as well as increase in the side lobes level by almost 10 dB. This chapter discusses a mmWave multiple-beam photonics BFN operating in the 37–43.5 GHz band (fractional bandwidth of 16%), for the implementation of which the Butler matrix (see **Figure 3**) is preselected (see section 3). In its scheme, to ensure the required phase shifts, optical delay lines of constant length are usually used [21]; therefore, prior to designing the specific BFN, the sensitivity analysis is also necessary.

In the process of simulation using MATLAB software, the sensitivity of the PAA’s NRP is examined for the example of a linear equidistant array of eight ideal isotropic elements designed for operation at the center (40.25 GHz) and two extreme (37.0 and 43.5 GHz) frequencies of the specified RF range. The BFN diagram was drawn based on the 8×8 Butler matrix according to **Figure 3** with the replacement of phase shifters with ideal equivalent delay circuits, in which the constant delay Δt was calculated at the center RF frequency f_c using the following well-known formula:

$$\Delta t = \Delta\varphi / (360f_c) \quad (8)$$

where $\Delta\varphi$ is the phase shift in degrees.

Table 2 lists the calculation results for phase shift (see **Figure 3**).

The results for MATLAB calculations of NRP using Eq. (7) at the center RF, lower RF, and upper RF in the azimuth angles range of $\pm 50^\circ$ from PAA broadside are shown in **Figures 9–11**, correspondingly.

Phase shift	22.5°	45.0°	67.5°	90.0°
Time delay	1.55 ps	3.1 ps	4.65 ps	6.2 ps

Table 2.
Time delays of the equivalent delay circuits of 8×8 Butler matrix.

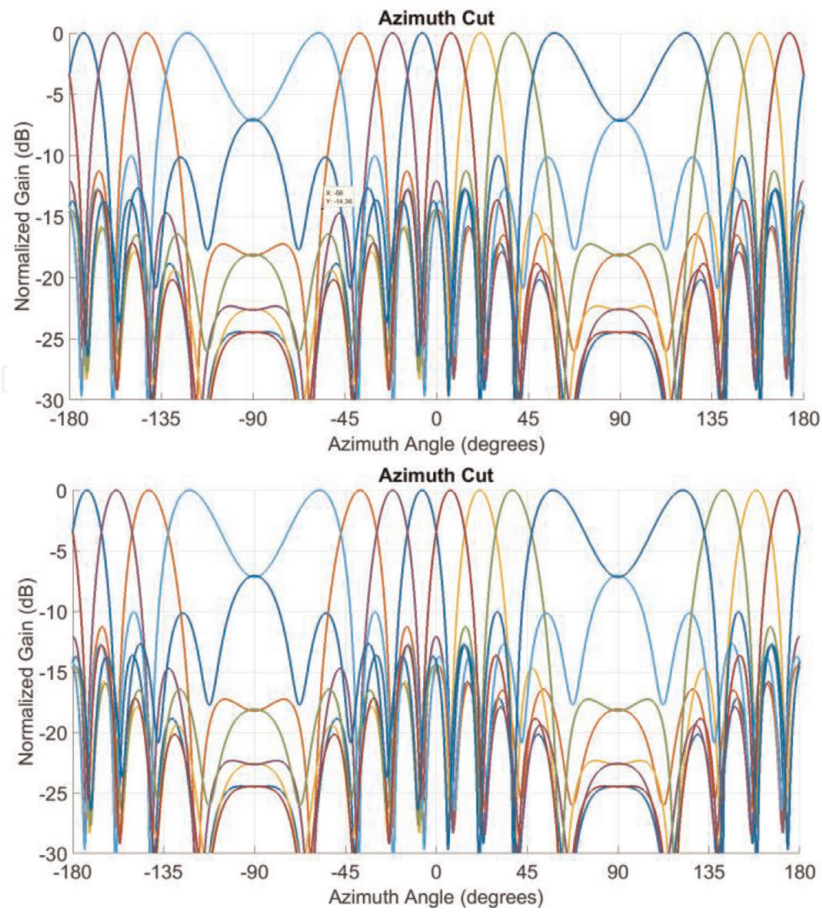


Figure 9. NRP at the center RF of 40.25 GHz using phase matrix (top) or time delay matrix (bottom).

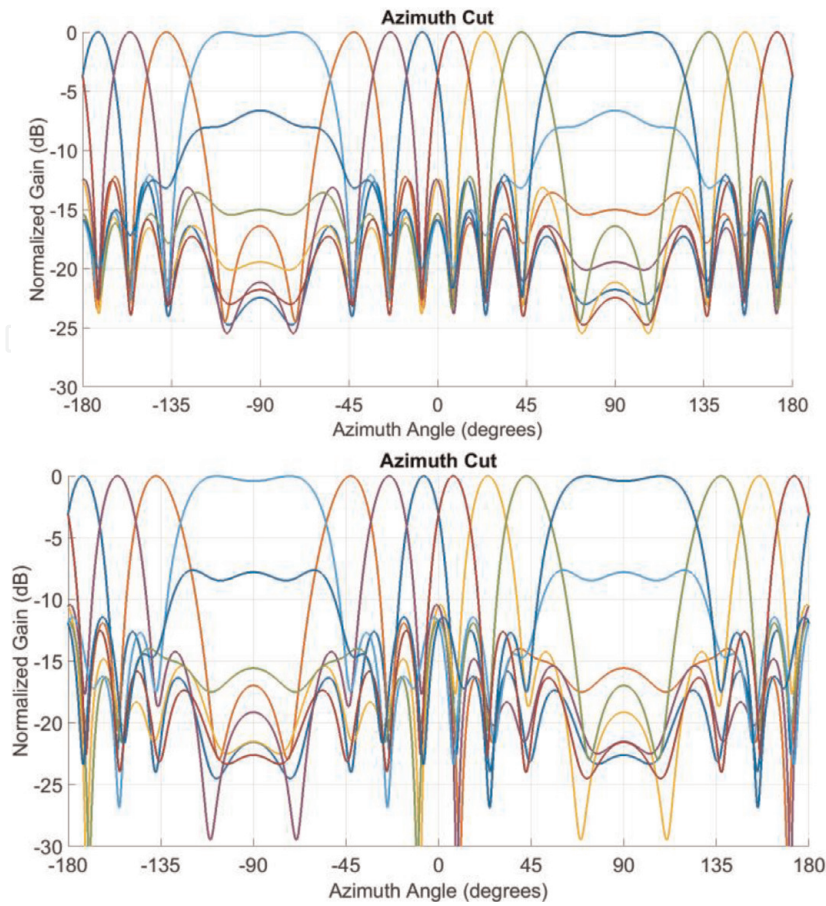


Figure 10. NRP at the lower RF of 37.0 GHz using phase matrix (top) or time delay matrix (bottom).

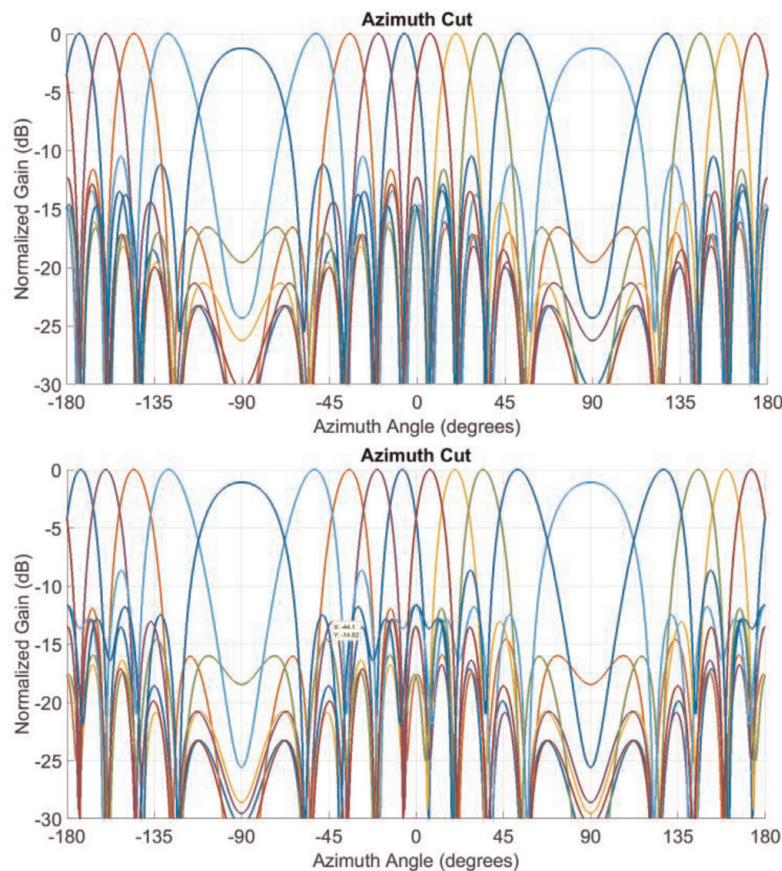


Figure 11. NRP at the upper RF of 43.5 GHz using phase matrix (top) or time delay matrix (bottom).

To summarize, the following outcomes could be concluded.

- According to [1], a Butler matrix provides a predetermined phase distribution at its outputs within the operating frequency band of its constituent components, such as quadrature hybrids and phase shifters. In it, when the RF deviates from the central one, the effect of beam squint is observed. The set of the beams narrows at the upper frequency and expands at the lower one, but the intersection point of the neighboring beams still remains at -4 dB from the maximum.
- When used in the matrix, some delay elements with the values given in **Table 2**, the effect of the beam squint is not observed, and the positions of the maxima do not change with RF, but the radiation patterns lose orthogonality, and the beams have a greater overlap at the lower frequency and less at the highest one.
- Despite visible deviations in the shape of radiation patterns, the simulation results demonstrate the possibility of using delay elements in the Butler matrix to ensure uniform coverage of the sector $\pm 50^\circ$ in the 37–43.5 GHz operating frequency range when the antenna elements are spaced through half the wavelength corresponding to the center frequency.

5. Design principles and ways of integrated photonics-based millimeter-wave array beamformers

In general, photonics-based BFNs for PAAs have many potential advantages over their electrical counterparts [18, 19, 22], such as small size, low weight, no

susceptibility to electromagnetic interference, and, especially, wide instantaneous bandwidth, and squint-free array steering while using TTD concept. This section first reviews the state of the art in mmWave photonic beamforming concepts and technologies and their potential application in multiple-beam antennas. Following it an updated schematic of multiple-beam mmWave array feed networks using photonics integrated circuit (PIC) of optical Butler matrix is proposed and modeling by well-known software tool VPIphotonics Design Suite [23].

To date several optical beamforming architectures have been proposed using different technological implementations [10] such as free-space optics, fiber optics, or integrated optics. Among them, integrated photonic beamformers (IPBF) are of particular interest from the point of view of compactness and moderate implementation costs [21, 24–28]. In addition, their attractiveness is expected to increase as the RF signal frequency increases up to mmWave. Today, a number of reviews and research papers are devoted to the study of building principles for 5G NR small cells in the mmWave band [13, 21, 29, 30]. **Table 3** highlights the main design principles and ways for mmWave IPBF.

The review of the referred sources allows us to conclude the following:

- The direction of mmWave IPBF is at the initial stage of its development. There are a small number of publications related to the research and development of IPBF in the field of telecommunications.
- There are two approaches to ensuring delays in an IPBF. The first is based on the transit time through the planar waveguide. The disadvantage of this method is the relatively large length of the waveguide, which leads to an attenuation of the signal and an increase in the dimensions of the beamformer. However, this method is often used due to the ease of implementation.
- The second approach involves the use of optical ring resonators. Its main disadvantage is narrowing the bandwidth with increasing group delay time, which leads to the necessity of cascading elements to obtain feasible delays. Nevertheless, with the help of ring resonators, it is possible to obtain an order of magnitude larger delay values.

No.	Time delay unit	Scheme	Bandwidth	Steering method, settling time	Delay range	Source
1	Integrated waveguide	Binary with 2×2 switches	Narrowband 42.7 GHz	Switchable, 4 bit, 20 ns	15.7 ps	[31]
2	Optical ring resonator	1×4 TTD binary tree	8.7 GHz at 90 GHz	Thermal tuning	172.4 ps	[32]
3	Integrated waveguide	2×2 Butler matrix	Approximately 200 MHz	Fixed	100 ps	[21]
4	Optical ring resonator	16×1 TTD binary tree	2.5 GHz	Thermal tuning	1200 ns	[33]
5	Integrated waveguide	8×8 Blass matrix	—	—	—	[33]
6	Integrated PLC waveguide	Independent phase and amplitude control, four channels	Narrowband, 60.8 GHz	Thermo-optic effect	±45°	[34]

Table 3.
Examples of mmWave IPBF.

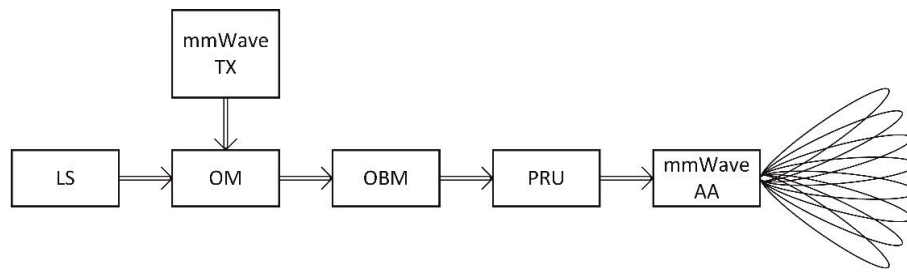


Figure 12.
Generalized block diagram of photonics-based mmWave multiple-beam array feed network.

- One of the most promising techniques for designing an RS's PAA is to use IPBFs based on a multiple-beam Butler matrix.

Analysis of the publications referenced in **Table 3** allows us to draw a generalized block diagram of photonics-based mmWave multiple-beam array feed network for downlink channel of RS, which is shown in **Figure 12**.

As follows from the Figure, the principal units are the laser sources (LS), optical modulators (OMs) performing the operation of electro-optical conversion, and the intensity of the output signal for which is controlled by the mmWave transmitter (TX). The output optical signals of the OMs are fed to a spatial distribution unit based on 8×8 optical Butler matrix. A photoreceiver unit (PRU) is connected to its outputs performing the operations of reverse optical-to-electrical conversion and amplification of the mmWave electrical signal to a level sufficient for reliable radio communication within the pico-cell of **Figure 2**, which is performed using the array antenna (AA). Note that the uplink channel between UT and RS is designed in a similar way and can be simplified using the reciprocity property of the Butler matrix.

5.1 Reference data for the simulation

In this work, the subject of the study is a mmWave multiple-beam array feed network, and the device of the study is an integrated optical Butler matrix. A tool for the computer simulation is the well-known commercial software VPIphotonics Design Suite™. In the course of the research, first of all, the accuracy of creating a mmWave 8×8 integrated OBM is checked. Then, the transmission quality of a mmWave multiple-beam array feed network using this OBM through the downlink channel for one of four sectors of the pico-cell RS (see **Figures 2** and **7**) is analyzed by the simulation in VPI and MATLAB software. **Table 4** lists the reference data for the integrated OBM under study and the setup for its characterization. In addition, **Table 5** lists the reference data for the array feed network under analysis.

5.2 CAD models and setups

According to the outcomes in the previous section, when analyzing with the help of MATLAB software, before modeling the integrated OBM using VPIphotonics Design Suite environment, it is worth checking the phase shifts provided by the equivalent delay elements based on integrated waveguides. **Figure 13** depicts the model that consists of one delay-less arm and the four arms with library models of TriPleX-based integrated waveguides ($n_g = 2.016$) providing phase shift of 22.5° , 45° , 67.5° , and 90° , correspondingly (see **Figure 3a** for the reference), and setup for the simulation experiments. In addition, there are two instrumental library models in the setup. The first one imitates optical transmitting module including library

Parameter	Value	
Number of optical inputs	8	
Number of optical outputs	8	
Band of RF carrier frequencies	37.5–41.0 GHz	
Input RF power	–11 to –26 dBm	
Material platform for IPBF	TriPleX (Si ₃ N ₄ /SiO ₂) [35]	
PIN photodiode	Responsivity	0.92 A/W
	Dark current	100 nA
	3 dB bandwidth	50 GHz
	Optical input power	<3 mW
Laser source	Optical carrier	193.1 THz
	Average power	50 mW
	Linewidth	10 kHz
Optical modulator	Principle	Electro-absorption
	Modulation type	Intensity, double sideband
	Spectral range	C band
	Modulation index	0.5
	Chirp factor	0

Table 4.
The reference data for the OBM under study and the setup for its characterization.

Parameter	Value
Overall number of mobile UTs in the pico-cell	72
Number of mobile UTs in one sector	18
Number of PAA sectors	4 (see Figure 7)
Number of PAA beams in one sector	6
Number of RF carrier frequencies	6
Band of RF carrier frequencies	38.0–40.5
Spacing of RF carrier frequencies	0.5 GHz

Table 5.
The reference data for the array feed network under analysis.

models of laser source and optical modulator EA controlled by RF generator tuning in the band of 37.5–41.0 GHz. The second one imitates optical receiving module including library models of PIN photodiode and RF network analyzer recording amplitude and phase RF signal distribution at the photodiode output. One can see their relevant parameters in **Table 4**.

Then, **Figure 14** depicts the model and setup of 8×8 OBM that in according to **Figure 3a** contains the models of quadrature optical hybrids (QOH) and library models of the straight waveguide as a phase shifter.

Due to the lack of a suitable library model in this software tool, QOH is designed as a so-called “galactic” module G, containing, in accordance with a typical circuitry of an electrical analog, library models of two optical X-couplers and two optical straight waveguides with 90° phase shift. Both elements are carried out based on

TriPleX technology. The internal scheme of the galactic module is presented in **Figure 15**. In addition, the setup of **Figure 14** includes two instrumental library models, which are the same as in **Figure 13**.

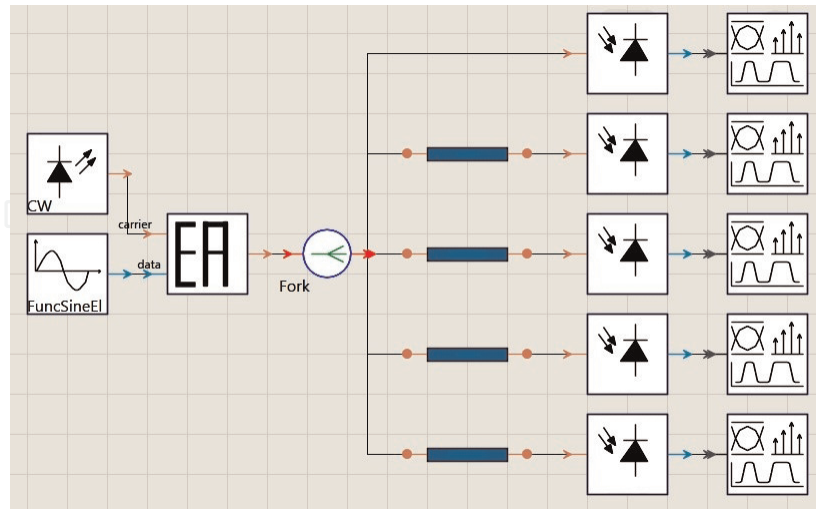


Figure 13.
 Equivalent delay elements of integrated OBM.

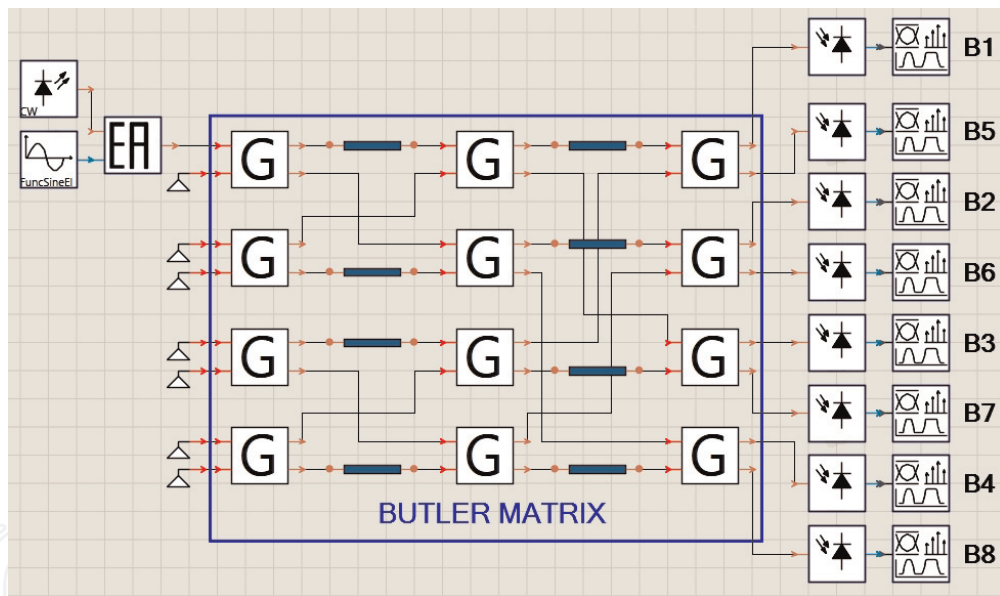


Figure 14.
 The model and setup for simulation of 8×8 PIC-based OBM.

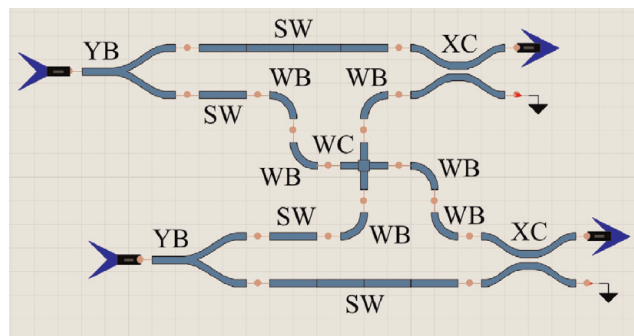


Figure 15.
 The internal scheme for the galactic module *G* of a quadrature optical hybrid.

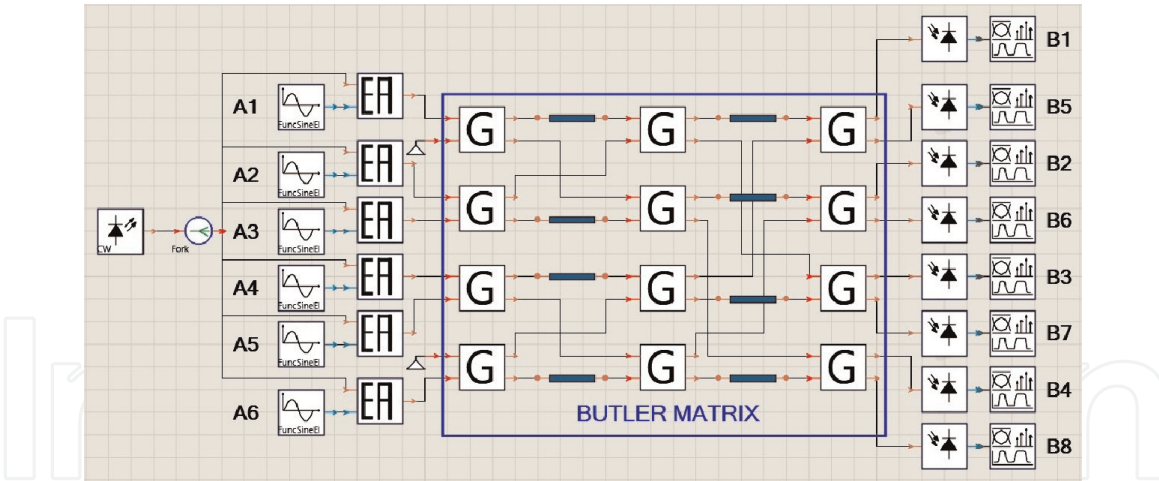


Figure 16.
The model and setup for simulation of mmWave multiple-beam array feed network.

The module of **Figure 15** contains a set of PIC library models, such as two Y-branches (YB), four straight waveguides (SW) including two SW for 90° phase shift, and two compensating SW with equivalent phase shift of 360° , six 90° waveguide bends (WB), one waveguide crossing element (WC), and two X-couplers (XC).

Finally, **Figure 16** depicts the model and setup for the mmWave multiple-beam array feed network under study that contains the model of 8×8 OBM (see **Figure 14**) with six inputs because as shown in subsection 3.1, the extreme beams generated by the Butler matrix (A2 and A7 in **Figure 3**) have a significantly greater width and less directivity than the others do (see **Figure 4**). In addition, there are two instrumental library models in the setup. The first one imitates optical transmitting module including library models of laser source and six optical modulators controlled by six RF generators, the RF carriers of which are allocated in the band of 38.0–40.5 GHz. The second one imitates optical receiving module including library models of eight PIN photodiodes and eight RF network analyzers recording amplitude and phase RF signal distributions at the photodiode outputs. One can see their relevant parameters in **Tables 4** and **5**.

5.3 Simulation results

First, a simulation experiment for the delay elements of PIC-based OBM (see **Figure 13**) was carried out. **Table 6** lists the results of phase error values for the center and two extreme frequencies of the RF generator.

Then, a simulation experiment for the PIC-based 8×8 OBM (see **Figure 14**) was carried out when the output of EA was alternately connected to each input of OBM, and at each point, the RF generator was sequentially tuned to the frequency of each

Reference phase shift		-22.5°	-45°	-67.5°	-90°
Equivalent lengths (mm)		0.215	0.437	0.662	0.883
Error value	At the center RF	-0.1°	-0.2°	-0.4°	-0.5°
	At the lowest RF	-1°	-2°	-3°	-4°
	At the upper RF	1°	2°	3.1°	4.1°

Table 6.
The simulation results of phase error values at the outputs of OBM under test.

downlink channel. **Table 7** exemplifies the simulation results of phase error values for channel A6 (see **Figure 16**) at the corresponding outputs.

Finally, a simulation experiment for the mmWave multiple-beam array feed network of **Figure 16** was carried out. **Figure 17** exemplifies the calculation results of the back-baffled normalized radiation patterns generated at the central and two extreme frequencies of the input RF band based on the data for the amplitude and

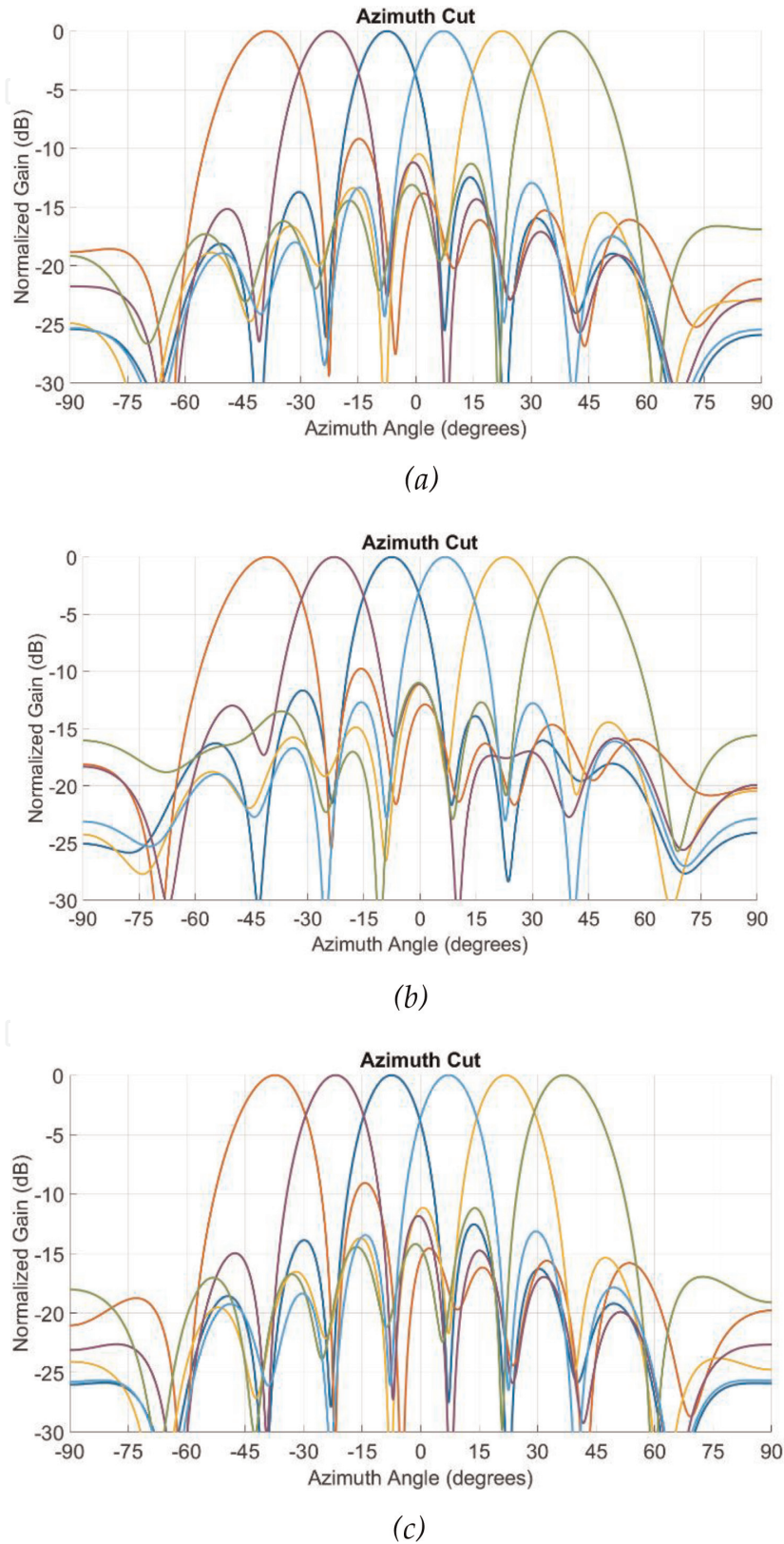


Figure 17. Normalized radiation patterns for the mmWave multiple-beam array feed network under test (a) at 39.5 GHz (b) at 38 GHz (c) at 40.5 GHz.

Input RF (GHz)	Output							
	B1	B5	B2	B6	B3	B7	B4	B8
39.0	10.4	9.5	9.1	8.3	7	6.1	5.6	4.8
38.0	0	0	0.5	0.5	0	0	0.4	0.5
40.5	-13.2	-12.7	-11	-9.8	-9.2	-8	-6.5	-5.2

Table 7.

The phase error values for the center and two extreme frequencies of the RF generators.

phase distribution of the waveforms at the outputs of the OBM, previously obtained using the calculation in the VPI software.

The following outputs can be derived from our study:

- According to **Table 6**, the phase error values for the tested delay elements of PIC-based OBM are not more than $\pm 4^\circ$.
- According to **Table 7**, the phase error values for 8×8 PIC-based OBM under test are not more than $+10^\circ/-13^\circ$.
- The assessment showed that the approximate area of the PIC is near 270 mm^2 , which is approximately 50 times less than the size of the electronic counterpart [36].
- According to **Figure 17**, the replacement of phase shifters with TTD elements led to a change in the position of the main lobe maximum and an increase in the relative level of side lobes. However, in comparison with the ideal radiation patterns of **Figures 9–11**, the azimuth position change does not exceed $\pm 2^\circ$, and the increase in the level is not more than 2 dB.

6. Conclusion

In the chapter, we explored and demonstrated the effectiveness of using reconfigurable multiple-beam array feed network based on millimeter-wave integrated photonics beamformers for the phased array antennas, which were known for a long time in the radar technique, in the small cells of the incoming fifth-generation mobile communication systems. The study was carried out using a specific example of designing an 8×8 optical Butler matrix-based photonics-steered beamforming network of a transmitting phased array antenna for a pico-cell remote station operating in the K_a/V-band with a 16% fractional bandwidth allocated as a promising one for future 5G systems. For this goal, we firstly reviewed the specialties of millimeter-wave photonics technique in 5G wireless networks of Radio-over-Fiber architecture. Then, to determine the input data for subsequent design, a theoretical background of array antenna beam steering using ideal models of phase shifters and true-time delay lines was presented. Comparison of the two most frequently used approaches to the design of multiple-beam antenna arrays based on Butler or Blass matrices showed the advantage of the first option for operation in the remote station of a 5G pico-cell.

A brief analysis of the available integrated millimeter-wave optical beamforming networks showed that the direction is at the initial stage of its development. A distinctive feature of the optical Butler matrix for designing beamformers is the

simple possibility of reconfiguring the antenna system in two directions: frequency reconfiguration due to the rearrangement of the RF synthesizer and spatial reconfiguration due to the introduction of a multichannel optical switch at the input. As a result of the simulation experiments performed using VPIphotonics Design Suite and MATLAB software, for both the integrated optical Butler matrix itself and the beamformer based on it, an acceptable quality of beams formation in a particular 5G pico-cell was obtained.

Acknowledgements

This work was supported by the Russian Foundation for Basic Research, Grants No. 17-57-10002 and No. 18-29-20083.

Conflict of interest


The authors declare the lack of “conflict of interest.”

Author details

Mikhail E. Belkin*, Dmitriy A. Fofanov, Tatiana N. Bakhvalova and Alexander S. Sigov
Scientific and Technological Center “Integrated Microwave Photonics”,
MIREA—Russian Technological University, Moscow, Russia

*Address all correspondence to: belkin@mirea.ru

IntechOpen

© 2019 The Author(s). Licensee IntechOpen. This chapter is distributed under the terms of the Creative Commons Attribution License (<http://creativecommons.org/licenses/by/3.0>), which permits unrestricted use, distribution, and reproduction in any medium, provided the original work is properly cited. 

References

- [1] Mailloux R. Phased Array Antenna Handbook. MA: Artech House, London; 2005. 496 p
- [2] Andrews JG, Buzzi S, Choi W, Hanly SV, Lozano A, Soong ACK, et al. What will 5G Be? IEEE Journal on Selected Areas in Communications. 2014;**32**(6):1065-1082
- [3] Waterhouse R, Novak D. Realizing 5G. IEEE Microwave Magazine. 2015;**16**(8):84-92
- [4] Chen S, Zhao J. The requirements, challenges and technologies for 5G of terrestrial mobile telecommunication. IEEE Communications Magazine. 2014; **52**(5):36-43
- [5] Munn J. Our 5G future: In the fast lane with numerical simulation. Microwaves & RF. Nov 16, 2016:48-50
- [6] Frenzel L. Making 5G happen. Microwaves & RF. 2017:1-5
- [7] Browne J. What role will millimeter waves play in 5G wireless systems? Microwaves & RF. 2018:38-42
- [8] Novak D, Waterhouse R. Emerging disruptive wireless technologies—Prospects and challenges for integration with optical networks. In: Optical Communication Conference and Exposition and the National Fiber Optic Engineers Conference (OFC/NFOEC); 17–21 March 2013. Anaheim, CA, USA: IEEE; 2013. pp. 1-3. DOI: 10.1364/OFC.2013.OTu3E.2
- [9] Novak D et al. Radio-over-fiber technologies for emerging wireless systems. IEEE Journal of Quantum Electronics. 2016;**52**(1):1-11
- [10] Belkin ME, Fofanov D, Golovin V, Tyschuk Y, Sigov AS. Design and optimization of photonics-based beamforming networks for ultra-wide mmWave-band antenna arrays. In: Array Pattern Optimization. United Kingdom, London: IntechOpen; 2018. pp. 47-67. Available from: <https://www.intechopen.com/online-first/design-and-optimization-of-photonics-based-beamforming-networks-for-ultra-wide-mmwave-band-antenna-a>
- [11] Boccardi F, Heath RW, Lozano A, Marzetta TL, Popovski P. Five disruptive technology directions for 5G. IEEE Communications Magazine. 2014; **52**:74-80
- [12] ITU. Final Acts of WRC-2015 World Radiocommunication Conference. Resolution 238. Geneva; 2016. pp. 296-298
- [13] Pi ZY, Khan F. An introduction to millimeter-wave mobile broadband systems. IEEE Communications Magazine. 2011;**49**(6):101-107
- [14] Bakhvalova T, Belkin M, Fofanov D. Advances in fiber-wireless network architecture approach to the next-generation communication systems. In: Proceedings of the seventh International Conference on Advances in Computing, Communication and Information Technology—CCIT; 27–28 October 2018. Rome, Italy; 2018. pp. 62-67
- [15] Rohwer AB, Desrosiers DH, BachW, Estavillo H, Makridakis P, Hrusovsky R. Iridium main mission antennas—A phased array success story and mission update. In: 2010 IEEE International Symposium on Phased Array Systems and Technology; 12–15 October 2010. Waltham, MA, USA: IEEE; 2010. pp. 504-511. DOI:10.1109/ARRAY.2010.5613319
- [16] Frank J. Bandwidth criteria for phased-array antennas. In: Oliner A,

- Knittel G, editors. Phased-Array Antennas. Dedham, MA: Artech House; 1972. pp. 243-253
- [17] Urlick VJ, McKinney JD, Williams KJ. Fundamentals of Microwave Photonics. New Jersey: Hoboken; 2015. 489 p
- [18] Matthews P. Practical photonic beamforming. In: International Topical Meeting on Microwave Photonics. MWP'99. Technical Digest (Cat. No. 99EX301); 17–19 November 1999. IEEE; 1999. pp. 271-274. DOI: 10.1109/MWP.1999.819701
- [19] Tur M. True time delay photonic beamforming: A review. In: IEEE International Conference on Microwaves, Communications, Antennas and Electronics Systems (COMCAS 2009). Tel Aviv; 2009
- [20] Belkin ME, Golovin V, Tyschuk Y, Sigov AS. Comparison of RF photonics-based beamformers for super-wide bandwidth phased array antennas. IOP Conference Series: Materials Science and Engineering. 2017;198:1-4
- [21] Liu H, Liu X, Effenberger F, Chand N, Qi X, Li G. Optical implementation of Butler matrix for hardware-efficient multiuser beamforming. IEEE Photonics Journal. 2018;10(2):1-8
- [22] Vidal B, Polo V, Corral JL, Martí J. Multibeam optical beamforming architectures for broadband wireless access networks. In: IST Mobile & Wireless Telecommunications Summit 2003; 15–18 June; Aveiro (Portugal); 2003
- [23] VPIphotonics Design Suite™. Available from: <https://www.vpi Photonics.com/Tools/DesignSuite/> [Accessed: 18 September 2019]
- [24] Fathpour S, Riza NA. Silicon-photonics-based wideband radar beamforming: Basic design. Optical Engineering. 2010;49(1):018201
- [25] Zhuang L et al. Novel ring resonator-based integrated photonic beamformer for broadband phased array receive antennas—Part II: Experimental prototype. Journal of Lightwave Technology. 2010;28(1): 19-31
- [26] Zhuang L et al. On-chip microwave photonic beamformer circuits operating with phase modulation and direct detection. Optics Express. 2014;22(14): 17079-17091
- [27] Roeloffzen CGH, Oldenbeuving R, Timens RB, et al. Integrated optical beamformers. In: Optical Fiber Communication Conference 2015; Los Angeles, CA, USA, ThA2; 2015. pp. 1-3
- [28] Alameh KE et al. Integrated microphotonic broadband smart antenna beamformer. In: Proceedings of the DELTA 2004. Second IEEE International Workshop on Electronic Design, Test and Applications; 28–30 January 2004; Perth, WA, Australia. IEEE; 2004. p. 208. DOI: 10.1109/DELTA.2004.10028
- [29] Roh W, Seol J-Y, Park J, et al. Millimeter-wave beamforming as an enabling technology for 5G cellular communications: Theoretical feasibility and prototype results. IEEE Communications Magazine. 2014;52(2): 106-113
- [30] Klein B, Jennings M, Hahnel R, Plettemeier D. Integrated Butler matrix and 1x4 antenna array for board-to-board communication in the mmWave-range. In: 2018 IEEE International Symposium on Radio-Frequency Integration Technology (RFIT); 15–17 August 2018; Melbourne, VIC, Australia. IEEE; 2018. DOI: 10.1109/RFIT.2018.8524054
- [31] Piqueras MA et al. Optically beamformed beam-switched adaptive

antennas for fixed and mobile broadband wireless access networks. IEEE Transactions on Microwave Theory and Techniques. 2006;54(2): 887-899

[32] Liu Y et al. Integrated optical beamforming network for millimeter wave communications. In: 2017 International Topical Meeting on Microwave Photonics (MWP); 23–26 October 2017. Beijing, China: IEEE; 2017. pp. 1-4. DOI: 10.1109/MWP.2017.8168704

[33] Roeloffzen C et al. Enhanced coverage through optical beamforming in fiber wireless networks. In: 2017 19th International Conference on Transparent Optical Networks (ICTON); 2–6 July 2017. Girona, Spain: IEEE; 2017. pp. 1-4. DOI: 10.1109/ICTON.2017.8025129

[34] Grosskopf G et al. Photonic 60-GHz maximum directivity beam former for smart antennas in mobile broad-band communications. IEEE Photonics Technology Letters. 2002;14(8): 1169-1171. DOI: 10.1109/LPT.2002.1022007

[35] Zhuang L, Marpaung D, Burla M, Beeker W, Leinse A, Roeloffzen C. Low-loss, high-index-contrast Si₃N₄/SiO₂ optical waveguides for optical delay lines in microwave photonics signal processing. Optics Express. 2011;19(23):23162-23170. DOI: 10.1364/OE.19.023162

[36] API Technologies. Available from: <https://www.apitech.com/brands/rf-solutions/weinschel-brand/> [Accessed: 18 September 2019]